HHS Public Access

Author manuscript

J Phys Chem Lett. Author manuscript; available in PMC 2019 October 18.

Published in final edited form as:

J Phys Chem Lett. 2018 October 18; 9(20): 6136–6142. doi:10.1021/acs.jpclett.8b02669.

Quasi-Resonance Signal Amplification By Reversible Exchange

Thomas Theis[a,b], **Nuwandi M. Ariyasingha**[c], **Roman V. Shchepin**[d], **Jacob Lindale**[b], **Warren S. Warren**[b], and **Eduard Y. Chekmenev**[*,c,e]

[a]Department of Chemistry, North Carolina State University, Raleigh, North Carolina, 27695-8204, United States

[b]Department of Chemistry, Duke University, Durham, North Carolina, 27708, United States

[c]Department of Chemistry, Integrative Biosciences (Ibio), Wayne State University, Karmanos Cancer Institute (KCI), Detroit, Michigan, 48202, United States

[d]Vanderbilt University Institute of Imaging Science (VUIIS), Department of Radiology and Radiological Sciences, Nashville, Tennessee, 37232-2310, United States

[e]Russian Academy of Sciences, Leninskiy Prospekt 14, Moscow, 119991, Russia

Abstract

Here we present the feasibility of NMR Signal Amplification by Reversible Exchange (SABRE) using radio-frequency irradiation at low magnetic field (0.05 T) in the regime, where the chemical shifts of free and catalyst bound species are similar. In SABRE, the ^{15}N-containing substrate and parahydrogen perform simultaneous chemical exchange on an Iridium hexacoordinate complex. Shaped Spin-Lock Induced Crossing (SLIC) radio-frequency pulse sequence followed by a delay is applied at QUASi-Resonance (QUASR) condition of ^{15}N spins of ^{15}N-enriched substrate. As a result of this pulse sequence application, ^{15}N z-magnetization is created from the spin-order of parahydrogen derived hyperpolarized hydrides. The repetition of the pulse-sequence block consisting of shaped radio-frequency pulse and the delay leads to the build-up of ^{15}N magnetization. The modulation of this effect by the irradiation frequency, pulse duration and amplitude, delay duration, and the number of pumping cycles was demonstrated. Pyridine-^{15}N, acetonitrile-^{15}N, metronidazole-$^{15}N_2$-$^{13}C_2$ substrates were studied representing three classes of compounds (five- and six-membered heterocycles and nitrile) showing the wide applicability of the technique. Metronidazole-$^{15}N_2$-$^{13}C_2$ is an FDA-approved antibiotic that can be injected in large quantities promising non-invasive and accurate hypoxia sensing. The ^{15}N hyperpolarization levels attained with QUASR-SABRE on metronidazole-$^{15}N_2$-$^{13}C_2$ were more than two-fold greater than with SABRE-SHEATH (SABRE in SHield Enables Alignment Transfer to Heteronuclei) demonstrating that QUASR-SABRE can deliver significantly more efficient means of SABRE hyperpolarization.

[*]Corresponding Author chekmenev@wayne.edu.

ASSOCIATED CONTENT

Supporting Information. Computation of ^{15}N signal enhancement and polarization values, photograph of the shaped RF pulse detected by the oscilloscope, Supporting Figures of the QUASR-SABRE effect, PDF.

This material is available free of charge via the Internet at http://pubs.acs.org.

Table of Contents Graphic

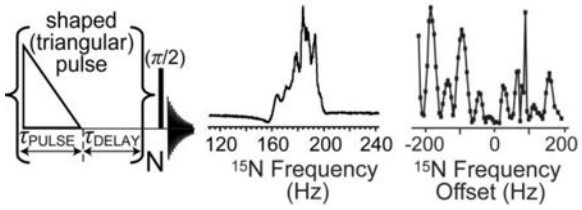

Conventional NMR relies on equilibrium thermal nuclear spin polarization P dictated by the Boltzmann distribution among Zeeman energy levels in dependence of the applied static magnetic field B_0. Although P can be boosted significantly by applying stronger magnetic field (because $P \propto B_0$), P is typically on the order of 10^{-5} to 10^{-6} for a conventional high-field NMR spectrometer (ca. 9.4 T) or MRI scanner (ca. 3 T) at room temperature, i.e. when the high temperature approximation holds. Hyperpolarization techniques increase P to the order of unity increasing NMR sensitivity increase by 4–5 orders of magnitude.[1–3]

Several hyperpolarization techniques exist.[1–3] Signal Amplification by Reversible Exchange (SABRE) is one of more recent techniques pioneered by Duckett and co-workers in 2009.[4–7] SABRE relies on simultaneous chemical exchange of parahydrogen (p-H_2) and to-be-hyperpolarized substrate (Figure 1a).[8] When the transient complex is formed, the parahydrogen symmetry is broken,[9] and the network of spin-spin couplings can enable transfer polarization from parahydrogen-derived hydrides to the nuclear spins of the substrate.[4–7] Two major groups of approaches have been developed for SABRE polarization transfer: the first group employs a matching static magnetic field B_{evo},[4, 10–13] and the second group applies radio-frequency (RF) pulse sequences,[14] to approach Level Anti-Crossings (LAC)[15–16] and induce polarization transfer. Both approaches have merit depending on the application. For biomedical applications, which represent the main driver for development of hyperpolarization technology,[2] the key is to achieve high degrees of polarization with the long lifetimes in a suitable biomolecular motif.[17] So far, approaches relying on static magnetic fields such as SABRE-SHEATH (SABRE in SHield Enables Alignment Transfer to Heteronuclei)[18–20] have been the most efficient for preparation of long-lived ^{15}N hyperpolarized spin states with exponential decay constant of more than 20 minutes[21] and P_{15N} exceeding 30%.[22–23]

One likely explanation as to why RF-based methods are lagging behind in the context of SABRE is the reliance on conventional high-field NMR spectrometers with small coils that only encompass a small fraction of the liquid sample in a 5 mm NMR tube,[14] which is continuously bubbled with p-H_2.[24] These factors result in major RF-inhomogeneities. In contrast, a previous approach used in hydrogenative Parahydrogen Induced Polarization (PHIP[9, 25–26]), employs low-field (*ca.* 5–50 mT) magnets and RF excitation coils,[27–32] which encompass the entire sample volume, sometimes in excess of 50 mL.[33–35] Moreover, the hardware behind such low-field devices is significantly less complex and less costly compared to that of the high-field NMR spectrometers.[17, 31–32, 35–36] Here it is demonstrated that these advantageous features can also be translated to SABRE.

RF-based polarization transfer such as Low-Irradiation Generation of High Tesla (LIGHT)-SABRE employs RF irradiation of the catalyst-bound substrate (Figure 1A), which typically has a chemical shift difference of 30–50 ppm with respect to the free substrate.[14, 37] Irradiation of the catalyst bound species allows for polarization transfer from p-H_2-derived hydrides.[14] When the complex dissociates, the ^{15}N nuclear spin polarization is preserved in the free substrate, because it is not affected by the frequency-selective RF pulses.[14] Achieving this frequency selective irradiation at high magnetic fields is trivial due to large chemical shift dispersion. For example, 50 ppm difference equals to ~2 kHz at 9.4 T. However, this difference vanishes at low magnetic fields: for example, 50 ppm difference equals 10 Hz at 0.05 T (the magnetic field employed in this Letter), and selective RF-excitation becomes challenging. We demonstrate that this challenge can be overcome through the use of quasi-resonance (QUASR) spin-lock induced crossing (SLIC)[38] irradiation to polarize ^{15}N spins from p-H_2-derived hydrides.

The QUASR-SABRE experiment (Figure 1B) is performed at 0.05 T magnetic field using previously described p-H_2 bubbling setup in a medium-walled 5-mm NMR tube.[24, 39–40] During p-H_2 bubbling a triangular-shaped pulse is applied for duration τ_{PULSE} followed by a delay period τ_{DELAY}. The process is repeated, and the net z-magnetization increases during this “rf-pumping” process. The resulting magnetization can be conveniently assessed by applying a broad-band excitation ($\pi/2$) RF pulse, Figure 1c. We compare the performance of this QUASR-SABRE approach with SABRE-SHEATH approach (Figure 1d), which has been employed previously to obtain record-high ^{15}N polarization in excess of 30%.[22–23]

The previously described SABRE-SHEATH setup,[39–40] ^{15}N RF coil and 0.05 T magnet have been employed here.[41] Samples of three substrates and IrIMes catalyst precursor in perdeuterated methanol were prepared as follows: pyridine-^{15}N/catalyst, ~20 mM/~1 mM, acetonitrile-^{15}N/catalyst, ~40 mM/~1–2 mM, metronidazole-$^{15}N_2$-$^{13}C_2$/catalyst, ~20 mM/~1 mM. All ^{15}N-enriched compounds were purchased from Isotec. The RF pulse sequences was coded and applied on Kea-2 NMR spectrometer (Magritek, New Zeeland) using Tomco RF amplifier. The employed Kea-2 spectrometer was operated in the signal averaging mode, where the signal is averaged during multi-scan acquisitions version being added. As a result, the signal integral value from multi-scan spectrum is similar to that acquired using 1-scan acquisition, e.g. the integral values of spectra shown in corresponding displays in Figures 2–4 can be compared directly without any scaling even though the spectra were recorded using different numbers of scans. A Three-layered mu-metal magnetic shield was employed (Magnetic Shield Corp., Bensenville, IL, P/N ZG-206). All data was acquired employing 75–80% parahydrogen prepared using home-built parahydrogen generator based on Sunpower cryo-chiller at a flow rate of 150 standard cubic centimeters per minute (sccm). For the SABRE experiments, the following conditions were used: 75 psi back-pressure and 70 sccm para-H_2 flow rate (Figure 1b and Figure 1d). The flow rate was maintained by via a mass flow controller (MFC, Sierra Instruments, Monterey, CA, P/N C100L-DD-OV1-SV1-PV2-V1-S0-C0).

Low-field detection of hyperpolarized (HP) compounds offers sufficient detection sensitivity in the context of NMR detection of HP states.[42] However, detection of thermal polarization is challenging due to low P even at high concentrations (see Supporting Information (SI) for

details). As a result, the quantification of ^{15}N enhancements (ε_{15N}) and polarization (P_{15N}) relied on signal to noise measurements (see SI for details) in order to determine the minimum values achieved.

^{15}N NMR spectra with high SNR were obtained for all three studied molecules: pyridine-^{15}N, acetonitrile-^{15}N, and metronidazole-$^{15}N_2$-$^{13}C_2$ using SABRE-SHEATH (Figure 2a, Figure 3a, and Figure 4a respectively) and QUASR-SABRE (Figure 2c, Figure 3c, and Figure 4c respectively). We note that while p-H_2 bubbling through the sample placed in 0.05 T leads to ^{15}N signal even without RF pulses (Figure 2b, Figure 3b and Figure 4b respectively), this ^{15}N signal is distinctly anti-phase,[14, 41, 43] and has significantly lower intensity compared to those obtained using SABRE-SHEATH and QUASR-SABRE protocols.

The key distinct feature of QUASR-SABRE phenomenon is strong RF offset frequency dependence: Figure 2d and Figure 4d demonstrate the dependence of the ^{15}N QUASR-SABRE signal for pyridine-^{15}N and metronidazole-$^{15}N_2$-$^{13}C_2$ respectively. Note that very small signal is obtained at the resonance frequency. The maximum intensity of ^{15}N QUASR-SABRE was compared to that of SABRE-SHEATH and is reported here as the ratio of ^{15}N QUASR-SABRE and SABRE-SHEATH signal, η. We find η of ~1.0 for pyridine-^{15}N, η of ~0.44 for acetonitrile-^{15}N, and η of (at least) ~2.4 for metronidazole-$^{15}N_2$-$^{13}C_2$. The relatively low η value for acetonitrile-^{15}N is in part explained by the fact that frequency optimization was not performed, and the data was recorded using the frequency offset parameter optimized for pyridine-^{15}N, which unfortunately did not provide a fair comparison. Based on the range of on the frequency optimization data for pyridine-^{15}N (Figure 2e) and for metronidazole-$^{15}N_2$-$^{13}C_2$ (Figure 4d), we estimate that this optimization may potentially yield an improvement of up ten-fold. We note that η value for metronidazole-$^{15}N_2$-$^{13}C_2$ assumes that both ^{15}N sites are hyperpolarized via SABRE-SHEATH and QUASR-SABRE protocols. While SABRE-SHEATH indeed yields hyperpolarization of both ^{15}N sites due to spin-relay of polarization at very low magnetic fields (the Earth's field (ca. 50 μT) and below), QUASR-SABRE may yield hyperpolarization of only one (N_3) site, Figure 4. If that is the case, then η would be effectively doubled to 4.8, because only one ^{15}N site contributes to the QUASR-SABRE signal (Figure 4c) versus two ^{15}N sites to the SABRE-SHEATH NMR signal (Figure 4a). We note that the Full Width at the Half-Height (FWHH) was approximately the same for SABRE-SHEATH and QUASR-SABRE NMR spectra for acetonitrile-^{15}N and metronidazole-$^{15}N_2$-$^{13}C_2$: Figure 3 and Figure 4 respectively, whereas QUASR-SABRE spectrum FWHH was approximately half of that for SABRE-SHEATH spectrum for pyridine-^{15}N (Figure 2c and Figure 2a respectively). The latter observation may in part explain pyridine-^{15}N η value, which is significantly lower than that of metronidazole-$^{15}N_2$-$^{13}C_2$.

All three molecules studies exhibited a clear and strong dependence of ^{15}N QUASR-SABRE signal on the duration of the pulse (τ_{PULSE}) and the duration of the delay (τ_{DELAY}): Figure S2a, Figure S3a and Figure S3b, Figure S4a and Figure S2b, Figure S3c, Figure S4b respectively. This strong dependence is likely due to the dynamics and kinetics of the substrate and p-H_2 exchange on the catalyst. When the τ_{PULSE} and τ_{DELAY} are in sync with

chemistry of exchange, the maximum QUASR-SABRE signal may be achieved. However, we note that QUASR-SABRE signal has very complex dependence on τ_{PULSE} and τ_{DELAY}. For example, the τ_{PULSE}-curves for acetonictrile-^{15}N are vastly different at τ_{DELAY} of 2 ms (Figure S3a) and τ_{DELAY} of 33 ms (Figure S3b). Future theoretical work is certainly warranted to study this complex behavior of QUASR-SABRE effect, which is outside the scope of this pioneering phenomenological report.

The second key feature of QUASR-SABRE effect allows for continuous “RF-pumping” of ^{15}N z-magnetization: Figure 2e, Figure 3d, and Figure 4e for the three studied compounds respectively. This fitting of the exponential dependence of the build-up processed yielded T_b of 0.5±0.05 s for acetonitrile-^{15}N, T_b of 1.26±0.02 s for pyridine-^{15}N, and T_b of 2.17±0.09 s for metronidazole-$^{15}N_2$-$^{13}C_2$. The T_b values correlate well with η values with R^2 of 0.93, Figure 5, suggesting that the build-up rate may be affecting the efficiency of QUASR-SABRE polarization process. A likely explanation of this observation in the contribution of the polarization destruction processes to T_b: when the destruction due to RF pulses is significant, T_b is reduced resulting in lower ^{15}N signals in a manner analogous to that of batch-mode Spin Exchange Optical Pumping (SEOP).[44–47] Further experimental and theoretical studies are certainly warranted in the future to maximize the efficiency of QUASR-SABRE approach described here.

All experiments were performed at room temperature (ca. 298 K). We note that the rf pumping of QUASR-SABRE process needs to be effectively matched to the chemical exchange dynamics in order to maximize the polarization transfer efficiency to yield the highest P_{15N} value. Therefore, it is expected that the optimal values of τ_{PULSE} and τ_{DELAY} (Figure S2, Figure S3, and Figure S4) would exhibit temperature dependence, because temperature modulates the rates of substrate and p-H_2 exchange. Moreover, it is entirely possible that optimum temperature (i.e. yielding the highest value of P_{15N}) may be significantly different from room temperature and may be different from optimal temperature of the SABRE-SHEATH process (note that the optimal SABRE-SHEATH temperature for pyridine-^{15}N and for metronidazole-$^{15}N_2$-$^{13}C_2$ corresponds to approximately room temperature, i.e. SABRE-SHEATH experiments were optimized with respect to temperature). As a result, some additional improvement in the maximum value of P_{15N} may be potentially expected for QUASR-SABRE process.

We have also investigated the dependence of the QUASR-SABRE signal on the amplitude of SLIC power amplitude. Figure S4c exhibits a plateau (with a range of approximately 6 decibels) with relatively steep slopes on both sides. This trend is expected, because LAC conditions are usually created in a relatively narrow power range.[15, 48]

Optimization of P_{15N} was not the goal of this report. Moreover, due to lack of direct ^{15}N signal reference (due to insufficient thermal equilibrium signal), we can only report the low limit of ε_{15N} and P_{15N} values. Metronidazole-$^{15}N_2$-$^{13}C_2$ QUASR-SABRE estimates were ε_{15N} ~$9*10^5$ and P_{15N} ~1.5% (these values are doubled if only N_3 site is hyperpolarized). Metronidazole-$^{15}N_2$-$^{13}C_2$ SABRE-SHEATH estimates were ε_{15N} ~$3.7*10^5$ and P_{15N} ~0.6%. Note these lower-limit estimates are in good agreement with P_{15N}~1.5% reported for SABRE-SHEATH under similar conditions using detection provided by high-resolution 9.4

T NMR spectrometer.[39–40] Pyridine-^{15}N lower-limit estimates were $\varepsilon_{15N} \sim 6.6*10^5$ and $P_{15N} \sim 1.1\%$ for both QUASR-SABRE and SABRE-SHEATH—in line with previous SABRE-SHEATH studies.[18–19] Acetonitrile-^{15}N lower-limit estimates were $\varepsilon_{15N} \sim 5.3*10^4$ and $P_{15N} \sim 0.09\%$ for QUASR-SABRE and $\varepsilon_{15N} \sim 1.2*10^5$ and $P_{15N} \sim 0.2\%$ for SABRE-SHEATH respectively. See SI for details.

With regards to the limitations of the QUASR-SABRE method, it remains to be seen if QUASR-SABRE is capable of hyperpolarization of long-range spin sites in the substrate compounds. Moreover, future systematic experimental and theoretical studies are certainly needed to further optimize the efficiency of QUASR-SABRE technique. For example, more advanced shaped forms (e.g. sine, exponential, trapezoid, etc.) and strategies (adiabatic pulses) can be envisioned.

In summary, radio-frequency based polarization transfer approach has been presented for polarization of ^{15}N sites. At least in some compounds, this method appears to be more efficient than the SABRE-SHEATH approach, which has already been shown to yield more than 30% ^{15}N polarization.[23] This is remarkable because in all previous demonstrations RF-SABRE approaches yielded significantly less polarization than static field matching / field cycling approaches. We hope that QUASR-SABRE may ultimately yield ^{15}N polarization of the order of unity for a wide range of biomolecules. The employed pulse-sequence is a shaped variant of SLIC pulse sequence,[38] which has the benefit of using low power levels. The applicability of this technique has been explored for three different types of compounds (six- and five-membered N-heterocycles and acetonitrile) including the antibiotic metronidazole. Metronidazole is an antibiotic that can be administered in large doses,[49] and contains the nitroimidazole moiety, which has been exploited in a wide range of molecular contrast agents for hypoxia sensing using position emission tomography (PET).[50–55] Therefore, metronidazole is a promising candidate as molecular probe for hypoxia imaging using HP MRI.[40]

Supplementary Material

Refer to Web version on PubMed Central for supplementary material.

Acknowledgments

Funding Sources

This work was supported by NSF under Grants CHE-1058727, CHE-1363008, CHE-1416268, and CHE-1836308. Research reported in this publication was also supported by the National Institute of Biomedical Imaging and Bioengineering of the NIH under R21EB025313 and 1R21EB020323, by National Cancer Institute under 1R21CA220137, and by DOD CDMRP under BRP W81XWH-12–1-0159/BC112431 and under W81XWH-15–1-0271.

REFERENCES

1. Goodson BM; Whiting N; Coffey AM; Nikolaou P; Shi F; Gust BM; Gemeinhardt ME; Shchepin RV; Skinner JG; Birchall JR, et al. Hyperpolarization Methods for MRS. Emagres 2015, 4, 797–810.
2. Nikolaou P; Goodson BM; Chekmenev EY NMR Hyperpolarization Techniques for Biomedicine. Chem. Eur. J 2015, 21, 3156–3166. [PubMed: 25470566]

3. Kovtunov KV; Pokochueva E; Salnikov OG; Cousin S; Kurzbach D; Vuichoud B; Jannin S; Chekmenev EY; Goodson BM; Barskiy DA, et al. Hyperpolarized NMR: D-DNP, PHIP, and SABRE. Chem. Asian J 2018, 13, 1857–1871.

4. Adams RW; Aguilar JA; Atkinson KD; Cowley MJ; Elliott PIP; Duckett SB; Green GGR; Khazal IG; Lopez-Serrano J; Williamson DC Reversible Interactions with Para-Hydrogen Enhance NMR Sensitivity by Polarization Transfer. Science 2009, 323, 1708–1711. [PubMed: 19325111]

5. Adams RW; Duckett SB; Green RA; Williamson DC; Green GGR A Theoretical Basis for Spontaneous Polarization Transfer in Non-Hydrogenative Parahydrogen-Induced Polarization. J. Chem. Phys 2009, 131, 194505. [PubMed: 19929058]

6. Atkinson KD; Cowley MJ; Duckett SB; Elliott PIP; Green GGR; López-Serrano J; Khazal IG; Whitwood AC Para-Hydrogen Induced Polarization without Incorporation of Para-Hydrogen into the Analyte. Inorg. Chem 2009, 48, 663–670. [PubMed: 19072592]

7. Atkinson KD; Cowley MJ; Elliott PIP; Duckett SB; Green GGR; Lopez-Serrano J; Whitwood AC Spontaneous Transfer of Parahydrogen Derived Spin Order to Pyridine at Low Magnetic Field. J. Am. Chem. Soc 2009, 131, 13362–13368. [PubMed: 19719167]

8. Rayner PJ; Duckett SB Signal Amplification by Reversible Exchange (SABRE): From Discovery to Diagnosis. Angew. Chem. Int. Ed 2018, 57, 6742–6753.

9. Bowers CR; Weitekamp DP Transformation of Symmetrization Order to Nuclear-Spin Magnetization by Chemical-Reaction and Nuclear-Magnetic-Resonance. Phys. Rev. Lett 1986, 57, 2645–2648. [PubMed: 10033824]

10. Shchepin RV; Truong ML; Theis T; Coffey AM; Shi F; Waddell KW; Warren WS; Goodson BM; Chekmenev EY Hyperpolarization of “Neat” Liquids by NMR Signal Amplification by Reversible Exchange. J. Phys. Chem. Lett 2015, 6, 1961–1967. [PubMed: 26029349]

11. Green RA; Adams RW; Duckett SB; Mewis RE; Williamson DC; Green GGR The Theory and Practice of Hyperpolarization in Magnetic Resonance Using Parahydrogen. Prog. Nucl. Mag. Res. Spectrosc 2012, 67, 1–48.

12. Hovener JB; Schwaderlapp N; Lickert T; Duckett SB; Mewis RE; Highton LAR; Kenny SM; Green GGR; Leibfritz D; Korvink JG, et al. A Hyperpolarized Equilibrium for Magnetic Resonance. Nat. Commun 2013, 4, 2946. [PubMed: 24336292]

13. Barskiy DA; Kovtunov KV; Koptyug IV; He P; Groome KA; Best QA; Shi F; Goodson BM; Shchepin RV; Truong ML, et al. In Situ and Ex Situ Low-Field NMR Spectroscopy and MRI Endowed by SABRE Hyperpolarization. ChemPhysChem 2014, 15, 4100–4107. [PubMed: 25367202]

14. Theis T; Truong M; Coffey AM; Chekmenev EY; Warren WS LIGHT-SABRE Enables Efficient in-Magnet Catalytic Hyperpolarization. J. Magn. Reson 2014, 248, 23–26. [PubMed: 25299767]

15. Pravdivtsev AN; Yurkovskaya AV; Zimmermann H; Vieth H-M; Ivanov KL Transfer of SABRE-Derived Hyperpolarization to Spin-1/2 Heteronuclei. RSC Adv 2015, 5, 63615–63623.

16. Ivanov KL; Pravdivtsev AN; Yurkovskaya AV; Vieth H-M; Kaptein R The Role of Level Anti-Crossings in Nuclear Spin Hyperpolarization. Prog. Nucl. Mag. Res. Spectrosc 2014, 81, 1–36.

17. Hövener J-B; Pravdivtsev AN; Kidd B; Bowers CR; Glöggler S; Kovtunov KV; Plaumann M; Katz-Brull R; Buckenmaier K; Jerschow A, et al. Parahydrogen-Based Hyperpolarization for Biomedicine. Angew. Chem. Int. Ed 2018, 57, 11140–11162.

18. Theis T; Truong ML; Coffey AM; Shchepin RV; Waddell KW; Shi F; Goodson BM; Warren WS; Chekmenev EY Microtesla SABRE Enables 10% Nitrogen-15 Nuclear Spin Polarization. J. Am. Chem. Soc 2015, 137, 1404–1407. [PubMed: 25583142]

19. Truong ML; Theis T; Coffey AM; Shchepin RV; Waddell KW; Shi F; Goodson BM; Warren WS; Chekmenev EY ^{15}N Hyperpolarization by Reversible Exchange Using SABRE-SHEATH. J. Phys. Chem. C 2015, 119, 8786–8797.

20. Colell JFP; Logan AWJ; Zhou Z; Shchepin RV; Barskiy DA; Ortiz GX; Wang Q; Malcolmson SJ; Chekmenev EY; Warren WS, et al. Generalizing, Extending, and Maximizing Nitrogen-15 Hyperpolarization Induced by Parahydrogen in Reversible Exchange. J. Phys. Chem. C 2017, 121, 6626–6634.

21. Theis T; Ortiz GX; Logan AWJ; Claytor KE; Feng Y; Huhn WP; Blum V; Malcolmson SJ; Chekmenev EY; Wang Q, et al. Direct and Cost-Efficient Hyperpolarization of Long-Lived

Nuclear Spin States on Universal 15N2-Diazirine Molecular Tags. Sci. Adv 2016, 2, e1501438. [PubMed: 27051867]

22. Barskiy DA; Shchepin RV; Coffey AM; Theis T; Warren WS; Goodson BM; Chekmenev EY Over 20% 15N Hyperpolarization in under One Minute for Metronidazole, an Antibiotic and Hypoxia Probe. J. Am. Chem. Soc 2016, 138, 8080–8083. [PubMed: 27321159]
23. Kidd BE; Gesiorski JL; Gemeinhardt ME; Shchepin RV; Kovtunov KV; Koptyug IV; Chekmenev EY; Goodson BM Facile Removal of Homogeneous SABRE Catalysts for Purifying Hyperpolarized Metronidazole, a Potential Hypoxia Sensor. J. Phys. Chem. C 2018, 122, 16848–16852.
24. Truong ML; Shi F; He P; Yuan B; Plunkett KN; Coffey AM; Shchepin RV; Barskiy DA; Kovtunov KV; Koptyug IV, et al. Irreversible Catalyst Activation Enables Hyperpolarization and Water Solubility for NMR Signal Amplification by Reversible Exchange. J. Phys. Chem. B 2014, 18 13882–13889.
25. Bowers CR; Weitekamp DP Para-Hydrogen and Synthesis Allow Dramatically Enhanced Nuclear Alignment. J. Am. Chem. Soc. 1987, 109, 5541–5542.
26. Eisenschmid TC; Kirss RU; Deutsch PP; Hommeltoft SI; Eisenberg R; Bargon J; Lawler RG; Balch AL Para Hydrogen Induced Polarization in Hydrogenation Reactions. J. Am. Chem. Soc 1987, 109, 8089–8091.
27. Waddell KW; Coffey AM; Chekmenev EY In Situ Detection of Phip at 48 mT: Demonstration Using a Centrally Controlled Polarizer. J. Am. Chem. Soc 2011, 133, 97–101. [PubMed: 21141960]
28. Coffey AM; Shchepin RV; Wilkens K; Waddell KW; Chekmenev EY A Large Volume Double Channel 1H-X RF Probe for Hyperpolarized Magnetic Resonance at 0.0475 Tesla. J. Magn. Reson 2012, 220, 94–101. [PubMed: 22706029]
29. Kovtunov KV; Truong ML; Barskiy DA; Koptyug IV; Coffey AM; Waddell KW; Chekmenev EY Long-Lived Spin States for Low-Field Hyperpolarized Gas MRI. Chem. Eur. J 2014, 20, 14629–14632. [PubMed: 25263795]
30. Kovtunov KV; Truong ML; Barskiy DA; Salnikov OG; Bukhtiyarov VI; Coffey AM; Waddell KW; Koptyug IV; Chekmenev EY Propane-D6 Heterogeneously Hyperpolarized by Parahydrogen. J. Phys. Chem. C 2014, 118, 28234–28243.
31. Coffey AM; Shchepin RV; Truong ML; Wilkens K; Pham W; Chekmenev EY Open-Source Automated Parahydrogen Hyperpolarizer for Molecular Imaging Using 13C Metabolic Contrast Agents. Anal. Chem 2016, 88, 8279–8288. [PubMed: 27478927]
32. Coffey AM; Shchepin RV; Feng B; Colon RD; Wilkens K; Waddell KW; Chekmenev EY A Pulse Programmable Parahydrogen Polarizer Using a Tunable Electromagnet and Dual Channel NMR Spectrometer. J. Magn. Reson 2017, 284, 115–124. [PubMed: 29028543]
33. Hövener J-B; Chekmenev EY; Harris KC; Perman W; Robertson L; Ross BD; Bhattacharya P Pasadena Hyperpolarization of 13C Biomolecules: Equipment Design and Installation. Magn. Reson. Mater. Phy 2009, 22, 111–121.
34. Hövener J-B; Chekmenev EY; Harris KC; Perman W; Tran T; Ross BD; Bhattacharya P Quality Assurance of PASADENA Hyperpolarization for 13C Biomolecules. Magn. Reson. Mater. Phy 2009, 22, 123–134.
35. Kadlecek S; Vahdat V; Nakayama T; Ng D; Emami K; Rizi R A Simple and Low-Cost Device for Generating Hyperpolarized Contrast Agents Using Parahydrogen. NMR Biomed 2011, 24, 933–942. [PubMed: 21845739]
36. Borowiak R; Schwaderlapp N; Huethe F; Lickert T; Fischer E; Bär S; Hennig J; Elverfeldt D; Hövener J-B A Battery-Driven, Low-Field NMR Unit for Thermally and Hyperpolarized Samples. Magn. Reson. Mater. Phy 2013, 26, 491–499.
37. Pravdivtsev AN; Yurkovskaya AV; Zimmermann H; Vieth H-M; Ivanov KL Enhancing NMR of Insensitive Nuclei by Transfer of SABRE Spin Hyperpolarization. Chem. Phys. Lett 2016, 661, 77–82.
38. DeVience SJ; Walsworth RL; Rosen MS Preparation of Nuclear Spin Singlet States Using Spin-Lock Induced Crossing. Phys. Rev. Lett 2013, 111, 5.

39. Shchepin RV; Jaigirdar L; Theis T; Warren WS; Goodson BM; Chekmenev EY Spin Relays Enable Efficient Long-Range Heteronuclear Signal Amplification by Reversible Exchange. J. Phys. Chem. C 2017, 121, 28425–28434.
40. Shchepin RV; Jaigirdar L; Chekmenev EY Spin-Lattice Relaxation of Hyperpolarized Metronidazole in Signal Amplification by Reversible Exchange in Micro-Tesla Fields. J. Phys. Chem. C 2018, 122, 4984–4996.
41. Shchepin RV; Barskiy DA; Coffey AM; Feldman MA; Kovtunova LM; Bukhtiyarov VI; Kovtunov KV; Goodson BM; Koptyug IV; Chekmenev EY Robust Imidazole-15N2 Synthesis for High-Resolution Low-Field (0.05 T) 15N hyperpolarized NMR Spectroscopy. ChemistrySelect 2017, 2, 4478–4483.
42. Coffey AM; Truong ML; Chekmenev EY Low-Field MRI Can Be More Sensitive Than High-Field MRI. J. Magn. Reson 2013, 237, 169–174. [PubMed: 24239701]
43. Kovtunov KV; Kidd BE; Salnikov OG; Bales LB; Gemeinhardt ME; Gesiorski J; Shchepin RV; Chekmenev EY; Goodson BM; Koptyug IV Imaging of Biomolecular NMR Signals Amplified by Reversible Exchange with Parahydrogen inside an MRI Scanner. J. Phys. Chem. C 2017, 121, 25994–25999.
44. Walker TG Fundamentals of Spin-Exchange Optical Pumping. Journal of Physics: Conference Series 2011, 294, 012001.
45. Nikolaou P; Coffey AM; Ranta K; Walkup LL; Gust B; Barlow MJ; Rosen MS; Goodson BM; Chekmenev EY Multi-Dimensional Mapping of Spin-Exchange Optical Pumping in Clinical-Scale Batch-Mode 129Xe Hyperpolarizers. J. Phys. Chem. B 2014, 118, 4809–4816. [PubMed: 24731261]
46. Nikolaou P; Coffey AM; Walkup LL; Gust BM; Whiting N; Newton H; Barcus S; Muradyan I; Dabaghyan M; Moroz GD, et al. Near-Unity Nuclear Polarization with an ‘Open-Source’ 129Xe Hyperpolarizer for NMR and MRI. Proc. Natl. Acad. Sci. U. S. A 2013, 110, 14150–14155. [PubMed: 23946420]
47. Barskiy DA; Coffey AM; Nikolaou P; Mikhaylov DM; Goodson BM; Branca RT; Lu GJ; Shapiro MG; Telkki V-V; Zhivonitko VV, et al. NMR Hyperpolarization Techniques of Gases. Chem. Eur. J 2017, 23, 725–751. [PubMed: 27711999]
48. Barskiy DA; Salnikov OG; Romanov AS; Feldman MA; Coffey AM; Kovtunov KV; Koptyug IV; Chekmenev EY NMR Spin-Lock Induced Crossing (SLIC) Dispersion and Long-Lived Spin States of Gaseous Propane at Low Magnetic Field (0.05 T). J. Magn. Reson 2017, 276, 78–85. [PubMed: 28152435]
49. Erickson SH; Oppenheim GL; Smith GH Metronidazole in Breast Milk. Obstet Gynecol 1981, 57, 48–50. [PubMed: 7454176]
50. Kizaka-Kondoh S; Konse-Nagasawa H Significance of Nitroimidazole Compounds and Hypoxia-Inducible Factor-1 for Imaging Tumor Hypoxia. Cancer Sci 2009, 100, 1366–1373. [PubMed: 19459851]
51. Procissi D; Claus F; Burgman P; Koziorowski J; Chapman JD; Thakur SB; Matei C; Ling CC; Koutcher JA In Vivo 19F Magnetic Resonance Spectroscopy and Chemical Shift Imaging of Tri-Fluoro-Nitroimidazole as a Potential Hypoxia Reporter in Solid Tumors. Clin. Cancer Res 2007, 13, 3738–3747. [PubMed: 17575240]
52. Komar G; Seppänen M; Eskola O; Lindholm P; Grönroos TJ; Forsback S; Sipilä H; Evans SM; Solin O; Minn H 18F-EF5: A New PET Tracer for Imaging Hypoxia in Head and Neck Cancer. J. Nucl. Med 2008, 49, 1944–1951. [PubMed: 18997048]
53. Hendrickson K; Phillips M; Smith W; Peterson L; Krohn K; Rajendran J Hypoxia Imaging with [F-18] FMISO-PET in Head and Neck Cancer: Potential for Guiding Intensity Modulated Radiation Therapy in Overcoming Hypoxia-Induced Treatment Resistance. Radiother. Oncol 2011, 101, 369–375. [PubMed: 21872957]
54. Masaki Y; Shimizu Y; Yoshioka T; Tanaka Y; Nishijima K.-i.; Zhao S; Higashino K; Sakamoto S; Numata Y; Yamaguchi Y, et al. The Accumulation Mechanism of the Hypoxia Imaging Probe “FMISO” by Imaging Mass Spectrometry: Possible Involvement of Low-Molecular Metabolites. Sci. Rep 2015, 5, 16802. [PubMed: 26582591]

55. Schwartz J; Grkovski M; Rimner A; Schöder H; Zanzonico PB; Carlin SD; Staton KD; Humm JL; Nehmeh SA Pharmacokinetic Analysis of Dynamic 18F-Fluoromisonidazole PET Data in Non–Small Cell Lung Cancer. J. Nucl. Med 2017, 58, 911–919. [PubMed: 28232611]

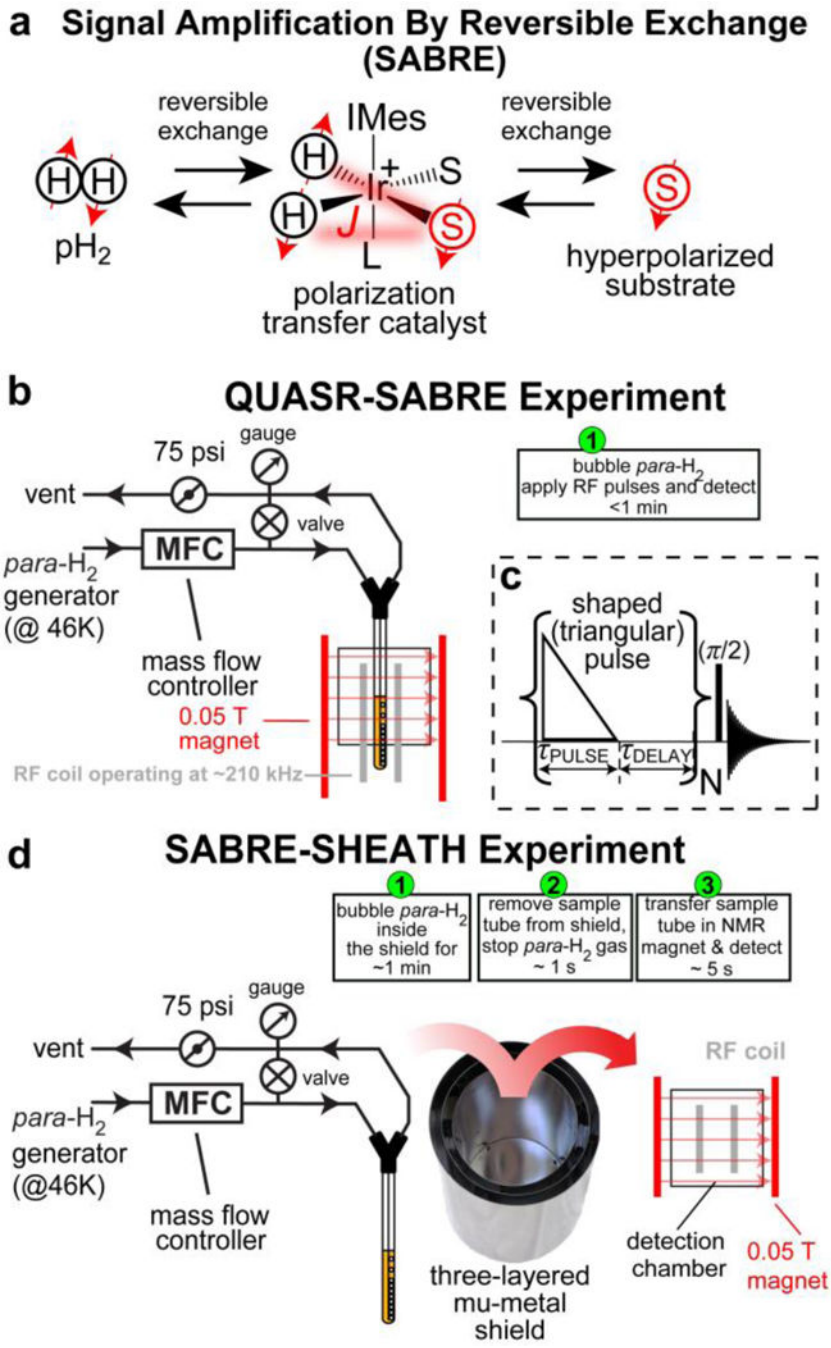

Figure 1.

a) The diagram of molecular exchange with p-H_2 in SABRE hyperpolarization. b) the experimental setup for QUASR-SABRE, c) the RF pulse sequence for QUASR-SABRE, d) corresponding experimental setup for SABRE-SHEATH experiment.

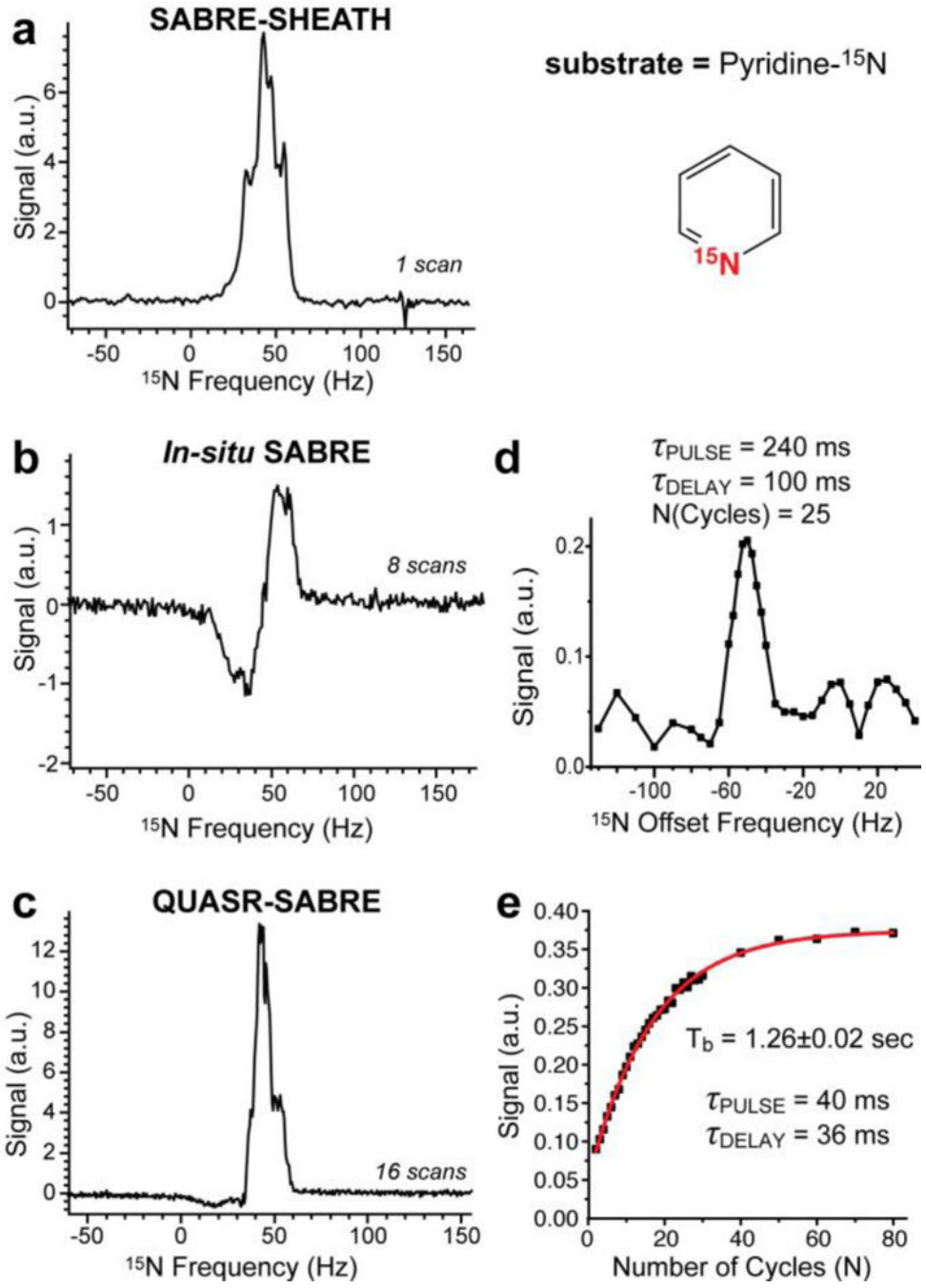

Figure 2.

Pyridine-^{15}N data. The other experimental conditions were as follows: 20 mM pyridine-^{15}N, 1 mM catalyst in CD_3OD. Note the width of the signal in displays b and d. a) the ^{15}N spectrum obtained after performing SABRE-SHEATH; b) The ^{15}N spectrum recorded using 90-degree excitation pulse when bubbling p-H_2 in situ of the 0.05 T magnet; c) the ^{15}N spectrum obtained after performing QUASR-SABRE; d) ^{15}N QUASR-SABRE signal dependence on the applied radio frequency offset from the actual resonance condition; e) the build-up of ^{15}N QUASR-SABRE signal as a function of the number of pumping cycles.

Note the individual spectra employed for figures in displays d and e were auto-phased, and the data is presented in the magnitude mode.

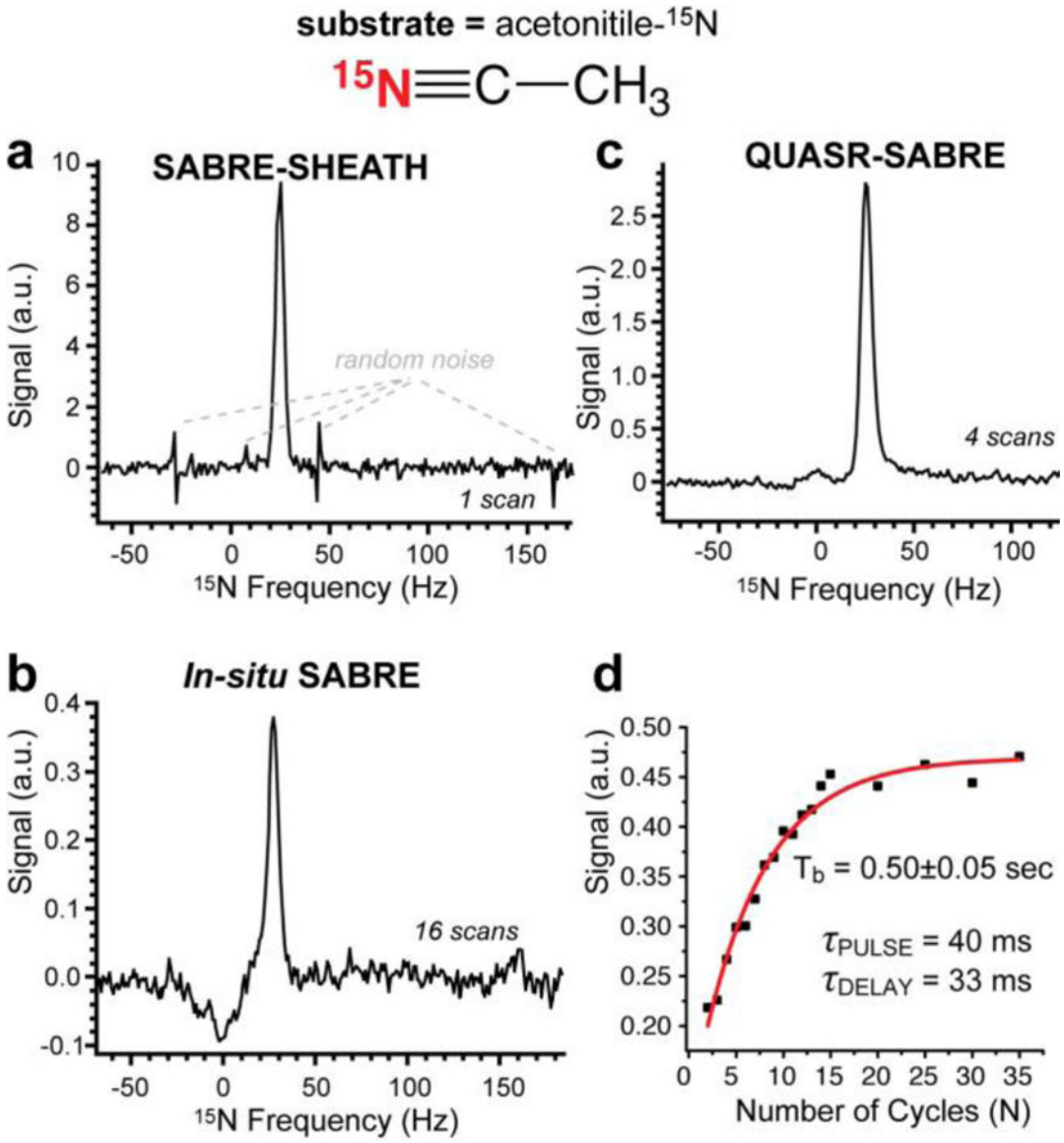

Figure 3.

acetonitrile-^{15}N data. The other experimental conditions were as follows: 40 mM acetonitrile-^{15}N, 1 or 2 mM catalyst in CD_3OD. Note the width of the signal in displays a and c is nearly the same as opposed to pyridine-^{15}N case. a) the ^{15}N spectrum obtained after performing SABRE-SHEATH; b) The ^{15}N spectrum recorded using 90-degree excitation pulse when bubbling p-H_2 in situ of the 0.05 T magnet; c) the ^{15}N spectrum obtained after performing QUASR-SABRE; d) the build-up of ^{15}N QUASR-SABRE signal as a function of the number of pumping cycles; Note the individual spectra employed for figures in display d were auto-phased, and the data is presented in the magnitude mode.

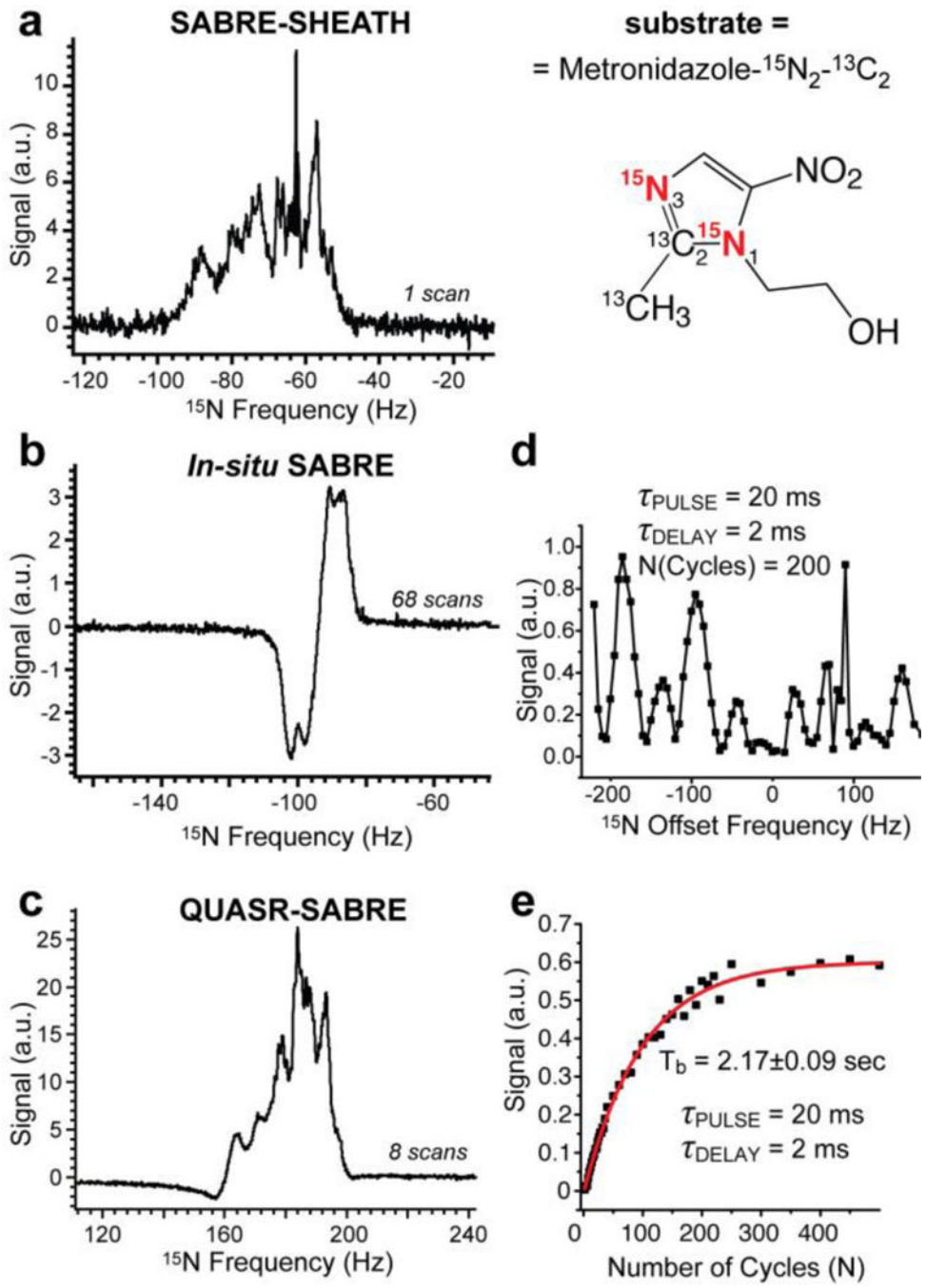

Figure 4.

Metronidazole-$^{15}N_2$-$^{13}C_2$ data. The other experimental conditions were as follows: ~20 mM metronidazole-$^{15}N_2$-$^{13}C_2$, 1 or 2 mM catalyst in CD_3OD. Note the width of the signal in displays a and c is nearly the same as opposed to pyridine-^{15}N case. a) the ^{15}N spectrum obtained after performing SABRE-SHEATH; b) The ^{15}N spectrum recorded using 90-degree excitation pulse when bubbling p-H_2 in situ of the 0.05 T magnet; c) the ^{15}N spectrum obtained after performing QUASR-SABRE; d) ^{15}N QUASR-SABRE signal dependence on the frequency of the applied RF shaped pulse; e) the build-up of ^{15}N QUASR-SABRE signal

as a function of the number of pumping cycles N. Note the individual spectra employed for figures in displays d and e were auto-phased, and the data is presented in the magnitude mode.

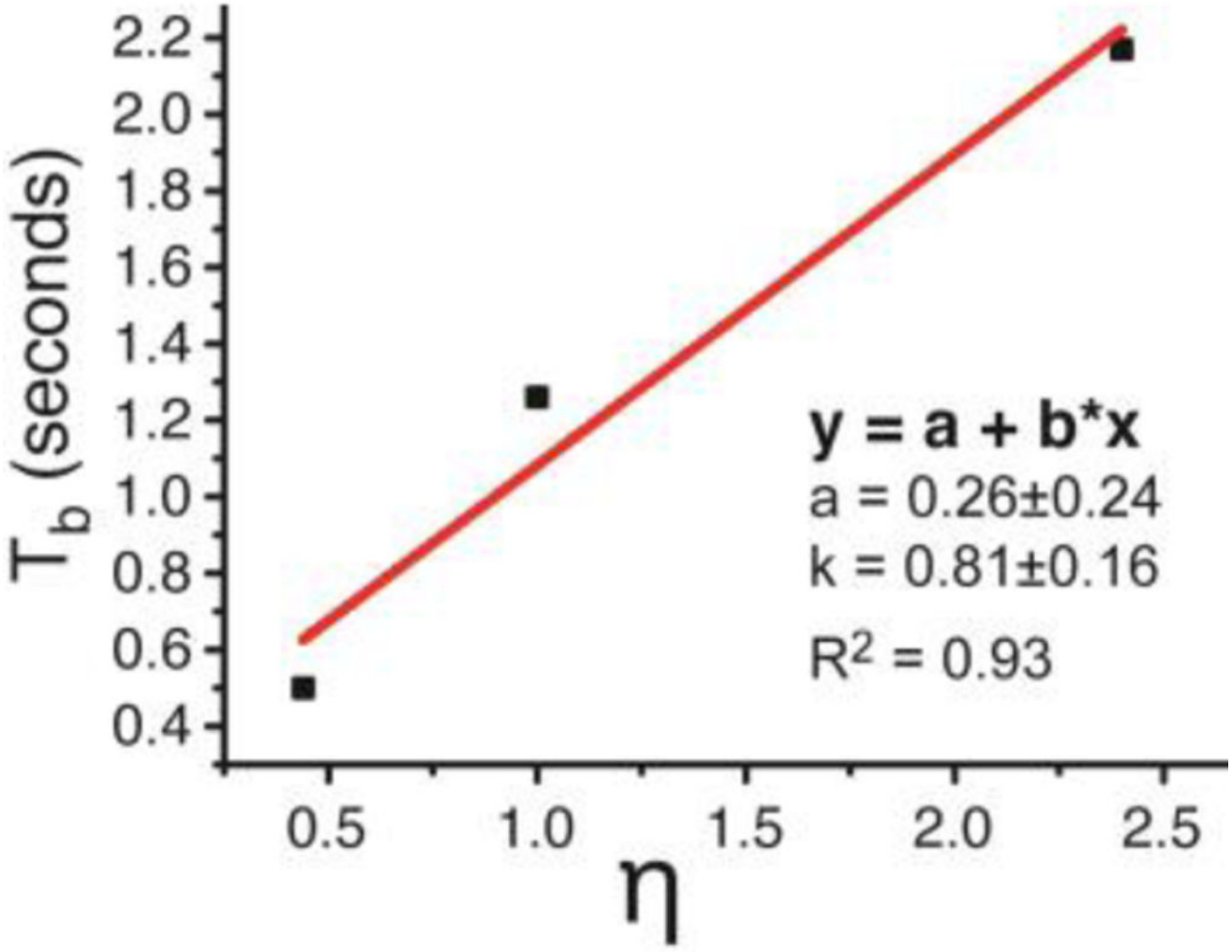

Figure 5.
Correlation plot of T_b and η for the three studied compounds.